Unified Sizing Model Approach for Radial and Axial Flux Permanent Magnet Machines

T. Carpi, M. Bonnet, S. Touhami, Y. Lefevre, J. F. Llibre.

***Abstract* -- Sizing equations of radial and axial electrical machines are developed. From these equations, the main geometrical parameters of the machines are obtained from the specifications and the loads. Analytical models of the open circuit and armature reaction fields are set up and associated to the sizing equations. This results in more accurate sizing equations. An axial and a radial flux motors are sized for the same loads and the same specifications to check the effectiveness of the sizing approach. Eventually Finite Element Analysis results validate the analytical models.**

***Index Terms*-- axial flux machines, radial flux machines, sizing model, sinusoidal machines.**

I. Introduction

Despite being more difficult to manufacture than its radial counterpart, Radial Flux Permanent Magnet (RFPM) motors, and with additional mechanical constraints, Axial Flux Permanent Magnet (AFPM) motors have very interesting characteristics [1]. However, it is still difficult to determine which electric motor topology is the most relevant for given specifications. That is why general purpose sizing equations have been developed for RFPM and AFPM motors [2][3]. The sizing equations are based on simple analytical expressions of electromagnetic quantities like the airgap magnetic flux density, flux per pole or torque [4][5]. In this paper, more accurate analytical models of the open circuit and the armature fields are developped to evaluate the electromagnetic quantities inside sizing approaches.

Complete analytical models of RFPM slotted motors are available now [6]. But these models are too complex. That is why analytical models of RFPM and AFPM slotless motors are considered [7][8][9]. Before applying these models, it is required the use of the Carter's coefficient.

Permanent magnet motors with Halbach array can produce high airgap magnetic flux density. Hence, they are good candidates for high specific power electric motors [10][11]. A RFPM motor with ideal Halbach array have been analytically modelized [12].

In this paper, the open field of RFPM and AFPM motors with ideal Halbach array are modeled analytically. Furthermore, these motors are supposed to have sinusoidal distribution of conductors and to be supplied by sinusoidal polyphase currents. Thus, the source of the armature reaction field is a sinusoidal surface current density on the stator bore [13]. Up to now armature reaction fields in RFPM and AFPM motors are often analytically modeled using magnetic vector potential [14]. The introduction of surface current density allows the use of magnetic scalar potential formulation.

For RFPM and AFPM, both open circuit and armature reaction fields analytical models will be associated with a sizing approach based on load concepts [13][15]. First the studied motors will be presented. Then the analytical models for RFPM and AFPM motors are described. To set up these models, slotless stators are considered, the magnetic permeability of iron is assumed infinite and the magnetic permeability of magnets equals unity. The modified unified sizing approach for RFPM and AFPM is developed before applying it to size AFPM and RFPM motors to show that it works well. That is why, for the simplicity of the presentation, the motors are sized not only with the same specifications but also with the same magnetic, electric and thermal loads. It is obvious that in real the practice, AFPM and RFPM motors may have the same specifications but do not have the same loads. As the introduction of simplified analytical models in a unified sizing approach is the one of the main contributions of this paper, FEA results are mainly intended to validate the open circuit and armature reaction field models of the sized RFPM and AFPM motors.

II. Studied Motors

The studied motors are surface mounted permanent magnet motors. They are supposed to have ideal Halbach array. They have both single airgap. The geometry of the RFPM motor is shown on Fig. 1 and the AFPM motor on Fig. 2. The geometrical parameters of both motors are given on Table I.

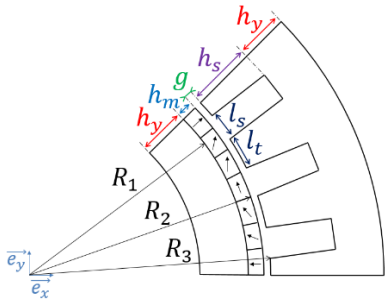

Fig. 1. Geometrical parameters of the RFPM motors [15].

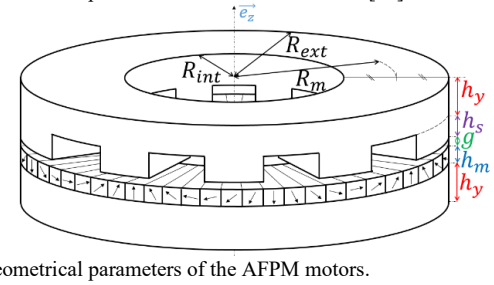

Fig. 2. Geometrical parameters of the AFPM motors.

T. Carpi, M. Bonnet, S. Touhami, Y. Lefevre and J. F. Llibre are with Laboratoire Plasma et Conversion d'Energie (LAPLACE), University of Toulouse, CNRS, 31000 Toulouse, France (email: {tcarpi, mbonnet, stouhami, lefevre, llibre}@laplace.univ-tlse.fr).

TABLE I
GEOMETRICAL PARAMETERS OF BOTH MOTORS

Parameter		RFPM	AFPM
h_m		Magnet radial thickness	Magnet axial thickness
h_y		Yoke radial thickness	Yoke axial thickness
h_s		Slot radial height	Slot axial height
l_s		Slot azimuthal width	Mean slot azimuthal width
l_t	A_t	Tooth azimuthal width	Mean tooth area
N_t		Number of slots or teeth	
L		Stack length	No signification
p		Number of pole pairs	

III. ANALYTICAL MODEL OF RFPM MOTOR

A. Open-circuit field model

The study domain of the open-circuit field is composed of two media: the airgap and the permanent magnets as illustrated in Fig. 3.

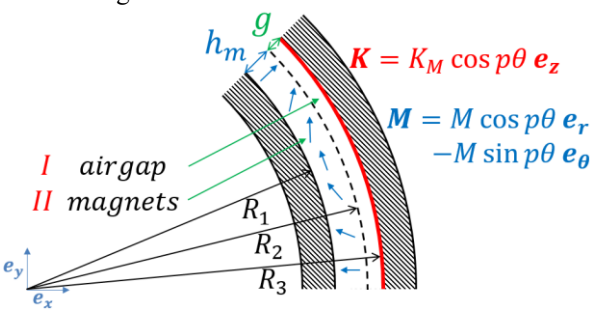

Fig. 3. Study domain of the RFPM motor open circuit field and armature field model.

The ideal Halbach magnetization distribution is given by [12]:

$$M_r(\theta) = M.\cos p\theta \quad (1)$$

$$M_\theta(\theta) = -M.\sin p\theta \quad (2)$$

Where M is the amplitude of magnetization. As there is no volume current density in the study domain, magnetic scalar potential (MSP) Ω can be used and static Maxwell equations lead to:

$$\Delta\Omega = \begin{cases} 0 & \text{in the airgap} \\ \operatorname{div} \boldsymbol{M} = \left(\frac{M}{r} - \frac{pM}{r}\right)\cos p\theta & \text{in the magnets} \end{cases} \quad (3)$$

The separation of variables applied to (3) in cylindrical coordinate system for the first harmonic gives the following expressions of magnetic scalar potential in airgap region I and magnet region II [12]:

$$\Omega^I = (a^I.r^p + b^I.r^{-p}).\cos p\theta \quad (4)$$

$$\Omega^{II} = (a^{II}.r^p + b^{II}.r^{-p} + c.r).\cos p\theta \quad (5)$$

Where $c = M/(1+p)$. The coefficients a^I, a^{II}, b^I and b^{II} are determined by boundary and interface conditions. As the permeability of iron is assumed infinite, the magnetic field is normal to the interfaces with iron. The interface conditions between the permanent magnets region II and the air region I are the continuity of the normal component of the magnet flux density B_n and the continuity of the tangential component of the magnetic field density H_t. Boundary and interface conditions are translated into MSP and then into a matrix system allowing to compute the coefficients. The final expression of the airgap radial magnetic flux density is thus:

$$B_r^{OC}(r,\theta) = B_M^{OC}(r).\cos p\theta$$

$$B_M^{OC}(r) = \mu_0 M.\frac{p}{p+1}\frac{\left(R_3^{2p} + r^{2p}\right).\left(R_2^{p+1} - R_1^{p+1}\right)}{r^{p+1}.\left(R_3^{2p} - R_1^{2p}\right)} \quad (6)$$

B. Armature reaction field model

The geometry of the study domain is still as the one shown on Fig. 3. However, the relative permeability of magnets is unity and magnetization of magnets is not taken into account. Thus, the study domain has only one medium.

The source of the armature reaction field is modeled as surface current density [6][13]. As the volume current density is null, the problem is also solved with the magnetic scalar potential Ω. The static Maxwell equations lead to:

$$\Delta\Omega = 0 \quad (7)$$

Using the separation of variables method, the following expression of MSP is obtained:

$$\Omega = (a.r^p + b.r^{-p}).\sin p\theta \quad (8)$$

The boundary conditions at radius $r = R_1$ and $r = R_3$ are:

$$H_\theta\big|_{r=R_3} = K_M \cos p\theta \quad (9)$$

$$H_\theta\big|_{r=R_1} = 0 \quad (10)$$

Translated into MSP, (9) and (10) lead to a matrix system allowing to compute coefficients a and b. The final expression of the radial magnetic flux density produced by the current sheet is:

$$B_r^{AR}(r,\theta) = B_M^{AR}(r).\sin p\theta$$

$$B_M^{AR}(r) = \mu_0.K_M.\frac{R_3^{p+1}}{r^{p+1}}.\frac{r^{2p} + R_1^{2p}}{R_3^{2p} - R_1^{2p}} \quad (11)$$

IV. ANALYTICAL MODEL OF AFPM MOTOR

AFPM motors require 3D models [9]. 3D analytical models even limited to the first harmonic is quite complex to handle in sizing approach. For the open circuit field, one of the very first analytical model of AFPM motor uses a 2D model in the azimuthal and axial directions (θ, z) [16]. In this section, two 2D analytical models for the open-circuit field and for the armature reaction field are presented. R_{int} and R_{ext} are the respective internal and external radius of the active parts of the studied motor and Fig. 4 shows the surface at the mean radius R_m and the (θ, z) frame where the models are set up.

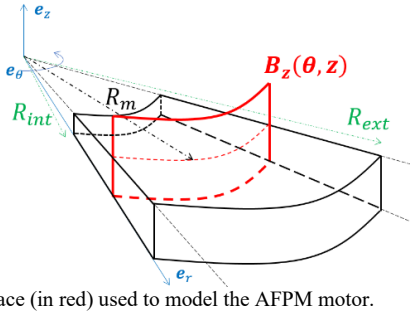

Fig. 4. 2D surface (in red) used to model the AFPM motor.

A. *Open circuit field 2D model*

The study domain is composed of two media, the airgap and the magnets, presented in Fig. 5 in a 2D (θ, z) frame. The ideal Halbach magnetization distribution is given by:

$$M_z(r,\theta,z) = M.\cos p\theta \quad (12)$$

$$M_\theta(r,\theta,z) = -M.\sin p\theta \quad (13)$$

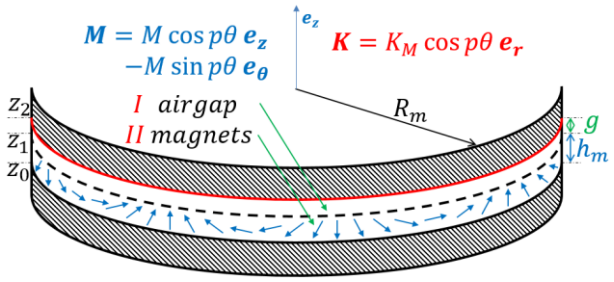

Fig. 5. Study domain of the AFPM motor open circuit field and armature reaction field model.

In terms of magnetic scalar potential Ω, Maxwell equations lead to:

$$\Delta\Omega = \begin{cases} 0 & \text{in } I \\ \text{div}\,\boldsymbol{M} = -\dfrac{pM}{r}\cos p\theta & \text{in } II \end{cases} \quad (14)$$

The separation of variables applied to (14) in cylindrical coordinates gives the following expressions of magnetic scalar potential in airgap region I and magnet region II:

$$\Omega^I = \left(a^I.\cosh\frac{p}{R_m}z + b^I.\sinh\frac{p}{R_m}z\right).\cos p\theta \quad (15)$$

$$\Omega^{II} = \left(a^{II}.\cosh\frac{p}{R_m}z + b^{II}.\sinh\frac{p}{R_m}z + c\right).\cos p\theta \quad (16)$$

Where $c = (R_m/p)M$. The coefficients a^I, a^{II}, b^I and b^{II} are determined by boundary and interface conditions. The magnetic field is normal to the interfaces with iron. Boundary and interface conditions are translated into MSP and then into a matrix system allowing to compute the coefficients. From Fig. 5 with $z_0 = 0$, $z_1 = h_m$, and $z_2 = h_m + g$, the expression of the airgap radial magnetic flux density at the mean radius is thus:

$$B_z^{OC}(\theta,z) = B_M^{OC}(z).\cos p\theta$$

$$B_M^{OC}(z) = \frac{\mu_0 M e^{-\frac{pz}{R_m}}\left(e^{\frac{2pz}{R_m}} + e^{\frac{2pz_2}{R_m}}\right)\left(e^{\frac{pz_1}{R_m}} - 1\right)}{e^{\frac{2pz_2}{R_m}} - 1} \quad (17)$$

B. *Armature reaction field 2D model*

The surface current density depends on the radial position. A general expression is taken as follows:

$$K(r,\theta) = K_M(r).cos(p\theta) \quad (18)$$

The surface current density must respect one major condition that is $\text{div}\,\boldsymbol{K} = 0$. This condition is naturally verified in RFPM. In the AFPM machine, this condition yields to:

$$K_M(r).r = cste \quad (19)$$

The 2D analytical model is set up at the mean radius R_m (Fig. 4). If K_m is the value of the magnitude at R_m, (19) leads to the magnitude at radial position r:

$$K_M(r) = \frac{K_m.R_m}{r} \quad (20)$$

As for the RFPM motor, the study domain of the armature field is composed only of one medium, its geometry is shown on Fig. 5.

The problem is also solved using a MSP formulation. The surface current density is taken as a boundary condition at $z = z_2$ as done for the RFPM machine. The Maxwell equations lead to:

$$\Delta\Omega = 0 \quad (21)$$

The separation of variables method brings to the following expression of MSP:

$$\Omega = \left(a.\cosh\frac{p}{R_m}z + b.\sinh\frac{p}{R_m}z\right).\sin p\theta \quad (22)$$

The boundary conditions at $z = z_1$ and $z = z_2$ are:

$$H_\theta\big|_{z=z_2} = K_M\cos p\theta \quad (23)$$

$$H_\theta\big|_{z=0} = 0 \quad (24)$$

Translated into MSP, (23) and (24) result in the final expression of the radial magnetic flux density:

$$B_z^{AR}(\theta,z) = \mu_0.K_M.\frac{\cosh\frac{p}{R_m}z}{\sinh\frac{p}{R_m}z_2}\sin p\theta \quad (25)$$

V. Main Electromagnetic Quantities

A. *Magnitudes of ideal sinewaves*

The open circuit magnetic flux density and surface current density at the stator bore are ideal sinewaves for both motors. For maximum operating torque [13]:

$$B(\theta,t) = B_M\cos(\omega t - p\theta) \quad (26)$$

$$K(\theta,t) = K_M\cos(\omega t - p\theta) \quad (27)$$

The corresponding vectors $\boldsymbol{B}$ and $\boldsymbol{K}$ are respectively carried by $\boldsymbol{e_r}$ and $\boldsymbol{e_z}$ for the RFPM machine, and $\boldsymbol{e_z}$ and $\boldsymbol{e_r}$ for the AFPM machine.

In the case of RFPM motors their magnitudes are constant. The stator bore is at radial position $(r = R_3)$ and the magnitude B_M is linked to the geometrical parameters by the open circuit model (6):

$$B_M = B_M^{OC}(R_3) \quad (28)$$

In the case of AFPM their magnitudes depend on the radial position r. The magnitude K_M is linked to the radial position by (20). At the stator bore $(z = z_2)$ and at the mean radius R_m, B_M is linked to the geometrical parameters by the open circuit model (17):

$$B_M(R_m) = B_M^{OC}(z_2) \quad (29)$$

To link the magnitude B_M to the radial position, a simple polynomial expression is chosen:

$$B_M(r) = a_0 r^2 + b_0 r + c_0 \quad (30)$$

(30) is a polynome of second degree which passes through the three points shown in Fig. 6. Several 3D studies brought us to choose $B_M(r)$ as illustrated in Fig. 6, where the following constants are chosen to be $c_1 = 0.6$ and $c_2 = 0.9$. Hence, coefficients a_0, b_0, c_0 can be computed.

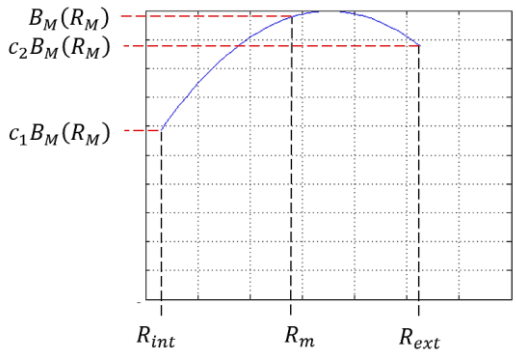

Fig. 6. Shape of $B_M(r)$ of the axial magnetic flux density at the stator bore ($z = z2$) of the AFPM motor.

B. *Torque model*

The general formula to compute torque is:

$$T(t) = \iint r.B(\theta,t).K(\theta,t).dS \quad (31)$$

The integral is done on the stator bore of each motor. This expression gives a torque that does not depend on time. For the RFPM motors the integral leads to [15]:

$$T = \pi R_3^2 L B_M K_M \quad (32)$$

By introducing the "root mean square values" B_{rms} and K_{rms}, the shear stress σ can be defined as [13][15]:

$$\sigma = B_{rms} K_{rms} \quad (33)$$

One can also define the rotor form ratio $\lambda = L/R_3$. Thus the torque can be simply expressed:

$$T = 2\pi\lambda R_3^3 \sigma \quad (34)$$

For the AFPM motor, considering (20), (31) leads to:

$$T = \pi R_m K_m . \int_{R_{int}}^{R_{ext}} r.B_M(r).dr = \pi R_m K_m I_{rbm} \quad (35)$$

The integral that appears in (35) is noted I_{rbm}. A new variable B_m is defined:

$$B_m = \frac{1}{(R_{ext} - R_{int})R_m} I_{rbm} \quad (36)$$

The torque for the AFPM motor can be simply expressed:

$$T = \pi R_m^2 (R_{ext} - R_{int}) B_m K_m \quad (37)$$

By introducing the "root mean square values", B_{rms} and K_{rms}, and the rotor form ratio:

$$\lambda = \frac{R_{ext} - R_{int}}{R_m} \quad (38)$$

The expression of the torque then becomes:

$$T = 2\pi\lambda R_m^3 \sigma \quad (39)$$

C. *Flux model*

The total magnetic flux density is the sum of the open circuit and the armature reaction magnetic flux densities. its magnitude is:

$$B_{TM} = \sqrt{(B_M^{OC})^2 + (B_M^{AR})^2} \quad (40)$$

As the leakage fluxes are neglected according to the pole surface S_p, the flux per pole is then written:

$$\phi_p = \iint_{S_p} B_{TM} cos(p\theta) dS \quad (41)$$

For the RFPM motor it is given by [13][15]:

$$\phi_p = \frac{2LR_3 B_{TM}}{p} \quad (42)$$

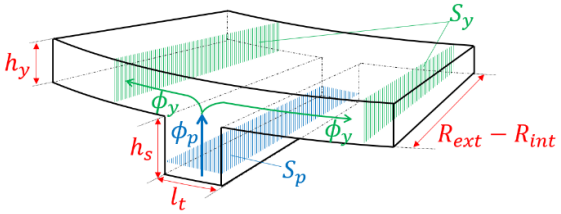

Fig. 7. Flux paths in the AFPM machine.

For the AFPM motor, the total field has a radial dependence. The flux per pole is then written:

$$\phi_p = \int_{-\pi/2p}^{\pi/2p} \int_{R_{int}}^{R_{ext}} r.B_{TM}(r).\cos p\theta \,.dr.d\theta \quad (43)$$

It is assumed that the total magnetic flux density inherits of the shape of the open circuit flux density (Fig. 6). After integration of (43), the I_{rbm} integral (35) can be used again. The flux per pole can be written using (29):

$$\phi_p = \frac{2}{p} I_{rbm} \frac{B_{TM}}{B_M(R_m)} \quad (44)$$

VI. UNIFIED SIZING EQUATIONS

The tool developed in [15] allows computing the main sizes of the RFPM motor knowing its specifications and its loads which are the input data given in Table II. The loads are chosen depending on the levels of the magnetic, electric and thermal manufacturing technologies at disposal. The output values are the sizes of the machine (Fig. 1). This paper proposes to extend the methodology presented in [15] to AFPM motors. The developed analytical models are used, instead of the analytical expressions used in [4] or [5], to calculate electromagnetic quantities more accurately.

A. *Association of open circuit field analytical models*

As in [15], the torque is deduced by the input data namely the mechanical power and the speed. Knowing the torque, the shear stress and the rotor form ratio, the bore radius, R_3, of the RFPM motor or the mean radius, R_m, of the AFPM motor are determined with torque models (34) and (39).

The open circuit models allow to determine the magnet thickness h_m. Indeed the input data give the airgap magnitude flux density B_M which are linked to the size of the motors by (6) and (28) for the RFPM motors and for the

AFPM motors by (17) and (29). The calculation of the magnet thickness with the open circuit field analytical model is not straightforward specially for the AFPM motors. The validation of this calculation is the main goal of the validation with finite element analysis (FEA).

B. Association of armature reaction field analytical models

The armature reaction field models allow to calculate the airgap reaction flux density B_M^{AR} by (11) and (25). The total magnetic flux density B_{TM} is computed from (40) allowing to evaluate the flux per pole with (42) and (44).

C. Flux balance

In the following, only the case of AFPM motor is developed. The case of RFPM motor is much more simple and can be found in [15] and Table III. The flux inside the yoke ϕ_y of AFPM motor is:

$$\frac{\phi_p}{2} = \phi_y = B_y S_y = B_y \times h_y(R_{ext} - R_{int}) \quad (45)$$

Which gives the yoke axial thickness:

$$h_y = \frac{\phi_p}{2\lambda R_m B_y} \quad (46)$$

TABLE II
INPUT DATA OF ASSESSMENT TOOL [15]

Mechanical specifications	**Thermal specifications**
Mechanical power, P_m	Ambient temperature, T_{amb}
Base rotational speed, N	Allowable heating, ΔT
Choice of load levels	**Geometrical parameters**
Magnetic shear stress, σ	Pole pairs, p
Max airgap magnetic radial flux density, B_M	Rotor form coefficient, λ Airgap ratio, x_g
Current density, j_{rms}	Winding head coefficients, k_{wh}
Magnetic flux densities allowed in stator teeth B_t and yoke B_y	Slot fill factor, k_{fill}

The total flux in the teeth ϕ_t, is the product of the average magnetic field in the teeth B_t and at the surface $N_t A_t$ through which this flux passes. With A_t the circular surface area of a tooth and N_t the number of teeth:

$$\phi_t = B_t N_t A_t \quad (47)$$

As leakage flux are neglected, the flux passing through all the teeth is equal to the flux of one pole times the number of poles:

$$\phi_t = 2p\phi_p \quad (48)$$

Combining equations (47) and (48), lead to the teeth area:

$$N_t A_t = \frac{2p\phi_p}{B_t} \quad (49)$$

D. Current balance

The linear current density for the AFPM motor is a function of the radial position and is taken at the mean radius:

$$A_{rms} = \frac{N_c I_{rms}}{2\pi R_m} = \frac{N_s I_{slot}}{2\pi R_m} \quad (50)$$

Where I_{slot} is the total current flowing through a slot, N_s is the number of slots and N_c is the total number of conductors. Considering that the slot has a rectangular shape:

$$N_s I_{slot} = N_s k_{fill} S_{slot} j_{rms} \quad (51)$$

$$S_{slot} = \frac{h_s A_s}{R_{ext} - R_{int}} = \frac{h_s A_s}{\lambda R_m} \quad (52)$$

Where S_{slot} is defined in (51) as the volume of one slot divided by the active length $R_{ext} - R_{int}$, and A_s is the circular surface left by the teeth area A_t. Then it comes:

$$h_s = \frac{S_{act} A_{rms}}{N_s A_s k_{fill} j_{rms}} \quad (53)$$

With S_{act} the surface area of the active parts, i.e.:

$$S_{act} = \pi(R_{ext}^2 - R_{int}^2) = 2\pi\lambda R_m^2 \quad (54)$$

It is also given by the relation:

$$S_{act} = N_t A_t + N_s A_s \quad (55)$$

E. Calculation of losses

The Joules losses are obtained according to the product $A_{rms} j_{rms}$ [15]:

$$P_j = q\rho_{Cu} S_{act} k_{wh} A_{rms} j_{rms} \quad (56)$$

Iron losses include eddy current losses, hysteresis losses and additional losses. These losses are evaluated using the Bertotti's formula:

$$P_{iron} = K_h B_{max}^2 f + K_c (B_{max} f)^2 + K_e (B_{max} f)^{1,5} \quad (57)$$

The K coefficients are given by the data of the iron magnetic sheet used for the motor. The frequency is calculated with the speed and the number of pole pairs $f = pN/60$. Table III gathers main unified sizing equations of RFPM motors [15] and the AFPM motors.

TABLE III
MAIN UNIFIED SIZING EQUATIONS

Parameter	RFPM	AFPM
λ	L/R_3	$(R_{ext} - R_{int})/R_m$
S_{act}	$2\pi\lambda R_3^2$	$2\pi\lambda R_m^2$
T	$S_{act} R_3 \sigma$	$S_{act} R_m \sigma$
ϕ_p	$2LR_3 B_{TM}/p$	$2.I_{rbm}.B_{TM}/p.B_M$
h_y	$\phi_p/2\lambda R_3 B_y$	$\phi_p/2\lambda R_m B_y$
h_s	$S_{act} A_{rms}/N_s l_s L k_{fill} j_{rms}$	$S_{act} A_{rms}/N_s A_s k_{fill} j_{rms}$
τ_{slot}	$N_s l_s/2\pi R_3$	$N_s A_s/S_{act}$
P_j	$q\rho_{Cu} S_{act} k_{wh} A_{rms} j_{rms}$	$q\rho_{Cu} S_{act} k_{wh} A_{rms} j_{rms}$

VII. APPLICATION OF THE MODEL

This application is only to show that the unified sizing equations work for both motors. Hence, the RFPM and AFPM motors have not only the same specifications but also the same loads. As the definition of the main input data is given in Table III, their values are gathered in Table IV.

TABLE IV
INPUT DATA OF THE SIZING MODEL

Input variable		
P_m	Mechanical Power	1 MW
N	Revolution per minute	8000 rpm
j_{rms}	Volume current density	10 A/mm^2
σ	Shear stress	80 000 Pa
B_m	Open circuit magnetic flux density	1.05 T
B_t	Magnetic flux density in teeth	1.5 T
B_y	Magnetic flux density in yoke	1.5 T
M	Magnetization of magnet	$875kA/m$
p	Number of pole pairs	4
λ_{AFPM}	AFPM rotor form coefficient	0.3
λ_{RFPM}	RFPM rotor form coefficient	1
x_g	Airgap ratio	0.01

Where x_g is the airgap ratio, $x_g = g/R_3$ for the RFPM motor and $x_g = g/R_m$ for the AFPM motor. The output data are the geometrical parameters defined in Table I, Fig. 1 and Fig. 2. Table V gives the output values for both motors.

TABLE V
OUTPUT DATA OF THE SIZING MODEL

Parameters	RFPM	AFPM
h_m	9.1 mm	17.6 mm
Main radius	$R_3 = 133.4$ mm	$R_m = 199.3$ mm
h_s	39.7 mm	37.3 mm
h_y	27.2 mm	38.2 mm
τ_{slot}	48 %	51 %
ST	12.23 Nm/kg	12.87 Nm/kg
SP	10.3 kW/kg	10.8 kW/kg
P_j	5.02 kW	4.03 kW
P_{iron}	4.65 kW	3.59 kW

Where τ_{slot} is the slot ratio (Table III), ST is the specific torque, SP is the specific power, P_j the Joule losses and P_{iron} the iron losses. These results show that knowing the specifications and the loads of the machines, their sizes and their performances can be computed. These values are shown to demonstrate that this unified sizing model allows comparing machine topologies. Of course in real practice the motors have not the same loads.

VIII. VALIDATION BY FEA

In order to validate the analytical models used in this sizing approach, the geometrical parameters in Table IV are taken as input of finite element analysis (FEA). The FEA of both RFPM and AFPM machine is performed on ANSYS Emag [17] in order to model the open circuit field. Only one pole is modeled due to the symmetries. Halbach array are modeled by seven permanent magnet segments as shown in Fig. 8 and Fig. 9. As in analytical models, the iron region is not taken into account. Two points of comparison are made in order to validate the model:

- The maximum magnetic flux in the airgap computed by FEA is compared to the one defined in input.
- The magnetic flux density useful to produce torque, i.e. B_r and B_z respectively for RFPM and AFPM machine, computed by FEA is multiplied by the theorical surface current density $K(r,\theta)$ and integrated to compute the torque.

A. *RFPM validation*

In the 2D FEA, as in the analytical model, the iron regions are replaced by normal flux boundary conditions.

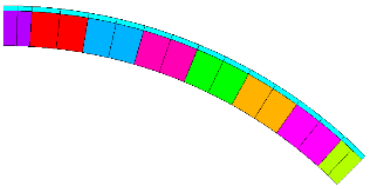

Fig. 8. Geometry of the RFPM machine 2D FEA model.

The FEA torque is computed from the airgap magnetic flux density distribution at the stator bore and the surface current density. Results and comparison between the model and the sizing model are gathered in Table VI.

B. *AFPM validation*

There are air regions above the magnets in the axial direction and besides the magnets in the radial direction as shown in Fig. 9. At interfaces with iron regions there are normal flux boundary conditions.

The axial magnetic flux density is extracted at the stator bore surface, it accounts for the radial and angular dependency of B_z.

The FEA magnetic flux density is multiplied by the theoretical surface current density. The integral on the active surface is carried out to calculate the torque with the formula:

$$T_{FEA} = \iint r.B_{z\,FEA}(r,\theta,z_2).K(r,\theta).dS \qquad (58)$$

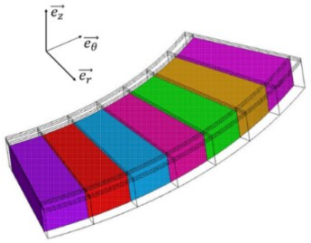

Fig. 9. Geometry of the AFPM machine 3D FEA model.

Results are gathered in Table VI. The error on the torque computation is about 1.9% and 1% respectively for AFPM and RFPM machine. The magnetic flux density wave along the stator bore is not a perfect sine as shown in Fig. 10. There is almost no error on the values calculated. There is almost no error when the fundamental magnitudes are compared. These results validate the 2D analytical models developed for RFPM and AFPM motors. The whole unified sizing equations have been validated by complete FE analyses but places are lacking to show them. This is the first step of a long campaign of validations. Anyway, the main contribution of the paper is the association of these simplified analytical models to the sizing equations. There were uncertainties for their accuracy. The results remove these uncertainties.

TABLE VI
COMPARISON BETWEEN SIZING MODEL AND FEA

		Torque $(N.m)$	Max magnetic flux at the stator bore (T)
AFPM	Sizing Model	1194	1.13
	ANSYS Emag	1217	1.1289
RFPM	Sizing Model	1194	1.05
	ANSYS Emag	1182	1.0478

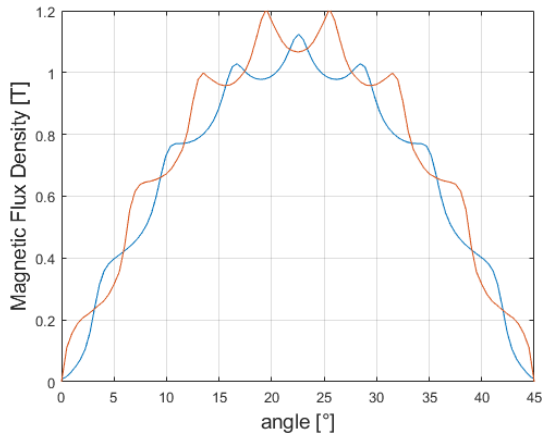

Fig. 10. Radial and axial magnetic flux density over one pole at the stator bore respectively for RFPM machine ($r = R_3$) and AFPM machine (at $z = z_2, r = R_m$).

IX. CONCLUSION

In this article, a unified sizing approach for RFPM and AFPM motors has been developed. This approach associates 2D simplified analytical models of the open circuit and armature reaction fields. The results show that the unified approach can be used to size quickly both machines if the specifications and the loads are known.

The association of analytical models in sizing approach is one of the major contribution of this paper. A first validation of this association has been done. The computation of the magnet thickness with the open circuit field model has been validated by FEA. Next step should have been the validation of the use of the open circuit and armature reaction field analytical models in the calculation of the total width of teeth and the yoke thickness. It has not been shown because it requires more places to present the results.

X. ACKNOWLEDGMENT

We would like to thank the Occitanie region for the financial support provided for the realization of this work.

XI. REFERENCES

[1] Gieras, J. F., Wang, R. J., Kamper, M. J. (2008). Axial flux permanent magnet brushless machines. Springer Science & Business Media.

[2] Huang, S., Luo, J., Leonardi, F., Lipo, T. A. (1998). A general approach to sizing and power density equations for comparison of electrical machines, IEEE Trans. on Ind. App., vol. 34, n 1.

[3] Huang, S., Luo, J., Leonardi, F., Lipo, T. A. (1999). A comparison of power density for axial flux machines based on general purpose sizing equations, IEEE Trans. on Energy Conv., vol. 14, n 2.

[4] Honsinger, V. B. (1987), Sizing equations for electric machinery, IEEE Trans. on Energy Conv., vol. EC-2, n 1.

[5] Slemon, G. R. (1994), On the design of high performance surface mounted PM motors, IEEE Trans. on Ind. App., vol. 30, n 1.

[6] Lubin, L., Mezani, S., Rezzoug, A. (2010), Exact analytical method for magnetic field computation in the air gap of cylindrical electrical machines considering slotting effects, IEEE Trans. on Mag., vol.46, n 4.

[7] Nogarede, B., Lajoie-Mazenc, M. & Davat, B. (1990), Modélisation analytique des machines à aimants à induits sans encoches, Revue de Phys. App., 25 (7), pp.707-720.

[8] Zhu, Z. Q., Howe, D. & Chan, C. C. (2002), Improved analytical model for predicting the magnetic field distribution in brushless permanent-magnet machines, IEEE Trans. on Mag., vol. 38, n 1.

[9] Carpi, T., Lefevre, Y., C. Henaux (2018), "Hybrid modeling method of magnetic field of axial flux permanent magnet machine", XXIII International Conference on Electrical Machines (ICEM), Alexandropouli, Greece.

[10] Yi, X., Yoon, A., Haran, K. S. (2017), Multi-physics optimization for high-frequency air-core permanent-magnet motor of aircraft application, IEEE Int. Elec. Mach. and Drives Conference (IEMDC), Miami, Florida, USA.

[11] Touhami, S. at al (2020), Electrothermal models and design approach for high specific power electric motor for hybrid aircraft, AeroSpace Europe Conf., Bordeaux, France.

[12] Xia, Z. P., Zhu, Z. Q., Howe, D. (2004), Analytical magnetic field analysis of Halbach magnetized permanent-magnet machines, IEEE Trans. on Mag., vol. 40, n 4.

[13] Touhami, S., Lefevre, Y., Llibre, J. F. (2018), Joint Design of Halbach. Segmented Array and Distributed Stator Winding. XXIII International Conference on Electrical Machines (ICEM), Alexandropouli, Greece.

[14] Liu, X., Hu, H., Zhao, J., Belahcen, A., Tang, L. (2016), Armature Reaction Field and Inductance Calculation of Ironless BLDC Motor, IEEE Trans. on Mag., vol. 52, n 2.

[15] Lefevre, Y., El-Aabid, S., Llibre, J. F., Henaux, C., Touhami, S. (2019). Performance assessment tool based on loadability concepts. International Journal of Applied Electromagnetics and Mechanics, 59(2), 687-694.

[16] Azzouzi, J., Barakat, G., Dakyo, B. (2005), Quasi-3D analytical modeling of the magnetic field of an axial flux permanent-magnet synchronous machine, IEEE Trans. on Energy Conv., vol. 20, n 4.

[17] ANSYS Mechanical APDL Low Frequency Electromagnetic Analysis 215 Guide. Release 17.2, document, Aug. 2016.

XII. BIOGRAPHIES

Theo Carpi was graduated from ENSEEIHT of Toulouse, France, in electrical engineering in 2016. He is currently pursuing the Ph.D. degree in electrical engineering at the Laboratory Plasma et Conversion d'Energie (LAPLACE), Toulouse.

Maxime Bonnet was graduated from ENSEEIHT of Toulouse, France, in electrical engineering in 2018. He is currently pursuing the Ph.D. degree in electrical engineering at the Laboratoire Plasma et Conversion d'Energie (LAPLACE), Toulouse.

Sarah Touhami was graduated from the "Ecole Nationale Superieur d'Electrotechnique, d'Electronique, d'Hydraulique et d'Informatique de Toulouse" (ENSEEIHT - France) in Electrical Engineering in 2015. She is currently pursuing the Ph.D. degree in electrical engineering at the "Laboratoire Plasma et Conversion d'Energie" (LAPLACE), Toulouse.

Yvan Lefevre was graduated from ENSEEIHT of Toulouse, France, in electrical engineering in 1983 and received the Ph.D. degree from the Institut National Polytechnique de Toulouse in 1988. He is currently working as a CNRS Researcher at Laboratoire Plasma et Conversion d'Energie (LAPLACE). His field of interest is the modeling of coupled phenomena in electrical machines in view of their design.

Jean-Francols Llibre has received the Ph.D. degree in Electrical Engineering from National Polytechnic Institute of Toulouse in 1997. He is a lecturer since 1998 and teaches electrical engineering in the University Institute of Technology of Blagnac near Toulouse since 2003. He joined the GREM3 electrodynamics research group of LAPLACE laboratory in 2010.